Applied Mathematics and Computation 217 (2011) 5041–5054

Contents lists available at ScienceDirect

Applied Mathematics and Computation

journal homepage: www.elsevier.com/locate/amc

Performance comparison of the NWF and DC methods for implementing high-resolution schemes in a fully coupled incompressible flow solver

F. Moukalled, A. Abdel Aziz, M. Darwish *

Department of Mechanical Engineering, American University of Beirut, P.O. Box 11-0236, Riad El Solh, Beirut 1107 2020, Lebanon

ARTICLE INFO

Keywords:
High-Resolution schemes
Coupled solver
Finite volume method

ABSTRACT

This paper reports on the use of the Normalized Weighting Factor (NWF) method and the Deferred Correction (DC) approach for the implementation of High-Resolution (HR) convective schemes in an implicit, fully coupled, pressure-based flow solver. Four HR schemes are realized within the framework of the NWF and DC methods and employed to solve the following three laminar flow problems: (i) lid-driven flow in a square cavity, (ii) sudden expansion in a square cavity, and (iii) flow in a planar T-junction, over three grid systems with sizes of 10^4, 5×10^4, and 3×10^5 control volumes. The merit of both approaches is demonstrated by comparing the computational costs required to solve these problems using the various HR schemes on the different grid systems. Whereas previous attempts to use the NWF method in a segregated flow solver failed to produce converged solutions, current results clearly demonstrate that both methods are suitable for utilization in a coupled flow solver. In terms of CPU efficiency, there is no global and consistent superiority of any method over another even though the DC method outperformed the NWF method in two of the three test problems solved.

1. Introduction

Solving flow problems using pressure based algorithms has been at the center of interest of CFD researchers for decades. Pressure based algorithms are classified as either segregated or coupled with the pressure–velocity coupling in the Navier Stokes equations accomplished by deriving a pressure equation from the mass conservation equation. In general, the pressure based segregated approach has been preferred since the formulation of the first Semi-Implicit Method for Pressure Linked Equations (SIMPLE) algorithm by the CFD group at the Imperial College [1] due to its simplicity of implementation and low memory requirement when compared to the coupled algorithm. The quick and wide acceptance of the segregated approach by the CFD community enticed researchers to extend this algorithm to a "family" of SIMPLE-like algorithms, which were found to share similar attributes as reported by the authors in [2]. The convergence rate of the SIMPLE-like family of algorithms is highly dependent on both the grid size and the under-relaxation factors. In general the denser the mesh, the more iterations and CPU time are needed. Also, segregated algorithms necessitate high under-relaxation to promote convergence.

Due to the significant advances in computer technology over the last two decades, the coupled algorithm started to re-capture the interest of researchers. The literature contains many early coupled algorithms that all proved to be competitive but suffered from a lack of robustness [3–7]. Recently, the authors of this article reported on a fully coupled algorithm

* Corresponding author.
E-mail address: darwish@aub.edu.lb (M. Darwish).

0096-3003/$ - see front matter © 2010 Elsevier Inc. All rights reserved.
doi:10.1016/j.amc.2010.07.052

Nomenclature

$a_P^\phi, a_F^\phi, \ldots$	coefficients in the discretized equation for ϕ
b_P^ϕ	source term in the discretized equation for ϕ
C	convective flux coefficient at control volume face
$\mathbf{d}_{PF}$	vector joining the grid points P and F
$\mathbf{D}_P$	the matrix **D** operator
g	geometric interpolation factor
J	total scalar flux across cell face
k	intercept in NVD
m	slope in NVD
$\dot{m}_f$	mass flow rate at control volume face f
p	pressure
P	main grid point
Q	general source term
RE	residual error
S	surface vector
u, v	velocity components in x- and y-direction, respectively
v	velocity vector
Ω_P	volume of the P cell

Greek symbols

ϕ	general scalar quantity
Γ	diffusion coefficient
μ	dynamic viscosity
ρ	fluid density

Subscripts

C	central grid point
D	downstream grid point
dc	deferred correction
f	refers to control volume face
F	refers to the F grid point
nb	refers to values at the faces obtained by interpolation between P and its neighbors
NB	refers to the neighbors of the P grid point
P	refers to the P grid point
U	upstream grid point

Superscripts

C	convection contribution
D	diffusion contribution
LO	low order scheme formulation
p	refers to pressure
u	refers to the u-velocity component
v	refers to the v-velocity component
$\sim$	refers to normalized variables

for the solution of incompressible flows [8,9] with acceleration rates of at least an order of magnitude higher than the ones achieved by the more popular segregated approach. Results also showed that the coupled method is nearly grid and under-relaxation independent.

In their algorithm [8,9] however, the convective flux in the momentum equations was discretized using the first order UPWIND scheme [10]. First-order schemes are numerically stable but highly diffusive. This numerical diffusion is desirable for numerical stability but often leads to highly inaccurate results and causes smearing of sharp gradients. To overcome this shortcoming and to increase the accuracy of the results predicted, researchers have developed a variety of higher-order schemes [11,12]. The difficulties associated with the development of reliable higher-order schemes stem from the conflicting requirements of accuracy, stability, and boundedness. Solutions predicted with high order schemes are more accurate than the first order upwind scheme and more stable than the second-order central difference scheme, but tend to provoke oscillations. To suppress oscillations, several techniques for developing HR schemes were presented leading to new families of High-Resolution (HR) schemes (i.e. high order bounded schemes), and the one adopted here is the composite flux limiter approach applied in the context of the Normalized Variable Formulation (NVF) [13]. The Deferred Correction (DC) procedure

[14] remained the preferred technique for the numerical implementation of these schemes, because it allows the use of codes originally intended for low order schemes by the addition of a source term that accounts for the difference in interpolated values between the high-resolution and low order scheme, at the price of a reduced convergence rate. A few examples of implicit methods of high resolution schemes were reported in the literature, namely the Downwind Weighing Factor (DWF) of Leonard and Mokhtari [15] and the Variable Curvature Factor (VCF) of Gaskell and Lau [16]. While the DWF suffers from some explicitness in its formulation, the main drawback of VCF is the important under-relaxation required to reach convergence. To overcome these issues and accelerate convergence, the Normalized Weighting Factor (NWF) method [17], which is fully implicit, was developed. While successful in solving for scalar transport equations, the NWF resulted in oscillations when dealing with flow problems.

The aim of any coupled solver is to accelerate convergence, therefore the effect of using high-resolution schemes implemented via the DC method on the convergence rate is of primary importance. To this end, the objectives of this paper are twofold: (i) to study the effect of implementing HR schemes using the DC method on the convergence of the coupled solver, and (ii) to extend the applicability of the NWF to flow problems by implementing it within the coupled solver and to compare its performance with the DC method. For this purpose, three flow test problems are solved using the SMART [16], OSHER [18], MINMOD [19], and MUSCL [20] HR schemes.

In what follows, the discretization procedure of the governing conservation equations, the coupled solvers, and the DC and NWF methods are briefly reviewed. Then the effect of using HR schemes applied using the DC approach and NWF method on the performance of the coupled algorithm is assessed by presenting results for the following three test problems on meshes of densities 10^4, 5×10^4 and 3×10^5 control volumes: (i) lid-driven flow in a square cavity, (ii) sudden expansion in a square cavity and (iii) flow in a planar T-junction.

2. The finite volume method

The conservation equations governing steady, laminar incompressible Newtonian fluid flow are given by

$$\nabla.(\rho\mathbf{v}) = 0, \tag{1}$$

$$\nabla\cdot(\rho\mathbf{v}\mathbf{v}) = \nabla\cdot(\mu\nabla\mathbf{v}) - \nabla\cdot p\mathbf{I}. \tag{2}$$

The above set of conservation equations can be cast into a general generic form as

$$\nabla\cdot(\rho\mathbf{v}\phi) = \nabla\cdot(\Gamma\nabla\phi) + Q. \tag{3}$$

The meanings of ϕ and Γ differ depending on the equation represented.

In the finite volume method, the domain is discretized by dividing it into a number of control volumes each associated with a main grid point placed at its geometric center. The discretization of the governing conservation equations is accomplished by integrating the general transport equation over the control volume to yield

$$\iint_\Omega \nabla\cdot(\rho\mathbf{v}\phi)d\Omega = \iint_\Omega \nabla\cdot(\Gamma\nabla\phi)d\Omega + \iint_\Omega Qd\Omega. \tag{4}$$

Then, using the divergence theorem, the first two volume integrals in Eq. (4) are transformed into surface integrals that are approximated by the trapezoidal rule over the faces contouring the control volume to yield

$$\sum_{f=nb(P)} (\rho\mathbf{v}\phi - \Gamma\nabla\phi)_f\cdot\mathbf{S}_f = Q_P\Omega_P. \tag{5}$$

Using appropriate interpolation schemes, the above semi-discretized equation is transformed to a fully discrete algebraic equation in the form

$$a_P^\phi\phi_P + \sum_{F=NB(P)} a_F^\phi\phi_F = b_P^\phi. \tag{6}$$

The discretization of the convection term is focal point of this paper. When the DC method is utilized, the convective flux is discretized using the upwind scheme. Then, an additive source term, that represents the difference in interpolated values between the upwind and the chosen HR scheme, is implemented. When using the NWF method, the HR scheme is implicitly implemented in the convective term. Details of this discretization are given when the two methods are described later.

3. The coupled algorithm

The discretization of the Navier Stokes equations will not be presented in full details in this paper. The complete discretization details, as well as some implementation tips for efficient computations, can be found in [8,9].

Unlike the segregated algorithm, the continuity and momentum equations are solved simultaneously in the coupled algorithm. Thus the need for predictor and corrector steps is removed. The only drawback of the coupled algorithm is the need for larger computer memory to store matrices that are nine times larger than those that result when implementing SIMPLE.

Without going into details, the discretized momentum equations in the x and y directions are of the following form:

$$\begin{cases} a_P^{uu}u_P + a_P^{uv}v_P + a_P^{up}p_P + \sum\limits_{F=NB(P)} a_F^{uu}u_F + \sum\limits_{F=NB(P)} a_F^{uv}v_F + \sum\limits_{F=NB(P)} a_F^{up}p_F = b_P^u, \\ a_P^{vu}u_P + a_P^{vv}v_P + a_P^{vp}p_P + \sum\limits_{F=NB(P)} a_F^{vv}v_F + \sum\limits_{F=NB(P)} a_F^{vu}u_F + \sum\limits_{F=NB(P)} a_F^{vp}p_F = b_P^v, \end{cases} \tag{7}$$

where the coefficient of the various terms are given by

$$\begin{aligned} &a_P^{uu} = J_f^C + \mu_f \frac{\mathbf{S}_f \cdot \mathbf{S}_f}{\mathbf{S}_f \cdot \mathbf{d}_{PF}}, \\ &a_P^{uu} = \sum_{F=NB(P)} a_F^{uu}, \quad a_P^{vv} = \sum_{F=NB(P)} a_F^{vv}, \\ &a_F^{uv} = 0, \quad a_F^{vu} = 0, \\ &a_P^{uv} = \sum_{F=NB(P)} a_F^{uv}, \quad a_P^{vu} = \sum_{F=NB(P)} a_F^{uv}, \\ &a_F^{up} = (1-g_f)S_f^x, \quad a_F^{vp} = (1-g_f)S_f^y, \\ &a_P^{up} = \sum_{f=nb(P)} g_f S_f^x, \quad a_P^{vp} = \sum_{f=nb(P)} g_f S_f^y, \\ &b_P^u = \sum_{f=nb(P)} \left[\nabla u \cdot \left(\mathbf{S}_f - \frac{\mathbf{S}_f \cdot \mathbf{S}_f}{\mathbf{S}_f \cdot \mathbf{d}_{PF}}\mathbf{d}_{PF}\right)\right], \quad b_P^v = \sum_{f=nb(P)} \left[\nabla v \cdot \left(\mathbf{S}_f - \frac{\mathbf{S}_f \cdot \mathbf{S}_f}{\mathbf{S}_f \cdot \mathbf{d}_{PF}}\mathbf{d}_{PF}\right)\right] \end{aligned} \tag{8}$$

and J_P^C is the convective coefficient. The value of J_P^C depends on the scheme used and whether the DC or NWF method is adopted.

The pressure equation is derived from the continuity equation by replacing the velocity at the interface with the Rhie–Chow approximation [21]. Its final discretized form is given by

$$a_P^{pp}p_P + a_P^{pu}u_P + a_P^{pv}v_P + \sum_{F=NB(P)} a_F^{pp}p_F + \sum_{F=NB(P)} a_F^{pu}u_F + \sum_{F=NB(P)} a_F^{pv}v_F = b_P^p, \tag{9}$$

where the coefficients are given by

$$\begin{aligned} &a_F^{pp} = \rho_f \frac{(\overline{\mathbf{D}_f}\mathbf{S}_f)\cdot\mathbf{S}_f}{\mathbf{S}_f \cdot \mathbf{d}_{PF}}, \\ &a_P^{pp} = \sum_{F=NB(P)} a_F^{pp}, \\ &a_F^{pu} = (1-g_f)S_f^x, \quad a_F^{pv} = (1-g_f)S_f^y, \\ &a_P^{pu} = \sum_{f=nb(P)} g_f S_f^x, \quad a_P^{pv} = \sum_{f=nb(P)} g_f S_f^y, \\ &b_P^p = \sum_{f=nb(P)} \rho_f\left(-\overline{\mathbf{D}_f \nabla p_f}\right)\cdot\mathbf{S}_f - \sum_{f=nb(P)} \rho_f\left(-\overline{\mathbf{D}_f}\nabla p_f\right)\cdot\left(\mathbf{S}_f - \frac{\mathbf{S}_f\cdot\mathbf{S}_f}{\mathbf{S}_f\cdot\mathbf{d}_{PF}}\mathbf{d}_{PF}\right). \end{aligned} \tag{10}$$

Combining the discretized momentum [Eq. (7)] and continuity [Eq. (9)] equations, a system of algebraic equations at each grid point P is obtained as

$$\begin{bmatrix} a_P^{uu} & a_P^{uv} & a_P^{up} \\ a_P^{vu} & a_P^{vv} & a_P^{vp} \\ a_P^{pu} & a_P^{pv} & a_P^{pp} \end{bmatrix} \begin{bmatrix} u_P \\ v_P \\ p_P \end{bmatrix} + \sum_{F=NB(P)} \begin{bmatrix} a_F^{uu} & a_F^{uv} & a_F^{up} \\ a_F^{vu} & a_F^{vv} & a_F^{vp} \\ a_F^{pu} & a_F^{pv} & a_F^{pp} \end{bmatrix} \begin{bmatrix} u_F \\ v_F \\ p_F \end{bmatrix} = \begin{bmatrix} b_P^u \\ b_P^v \\ b_P^p \end{bmatrix}. \tag{11}$$

In conclusion, the overall coupled algorithm can be summarized as follows:

1. Start with the nth iteration values $\left(\dot{m}_f^{(n)}, \mathbf{v}^{(n)}, p^{(n)}\right)$.
2. Assemble and solve the momentum and continuity equation to get updated values of velocity and pressure.
3. Assemble the mass flux at the interface using the Rhie–Chow interpolation.
4. Solve all other scalar equations sequentially.
5. Return to the first step and repeat until convergence.

In the following sections, HR schemes are described and then detailed discretization of the convective flux is presented.

4. High-resolution schemes

The convection flux in a conservation equation is given by

$$J_f^C = \dot{m}_f \phi_f. \tag{12}$$

In the Navier Stokes' equations the scalar ϕ represents a velocity component. Even though CFD researchers may be satisfied with the low order upwind scheme in discretizing the convective flux due to its robustness, boundedness, and implementation simplicity; using a robust high order scheme is always desirable. Second order schemes like QUICK and SOU, as well as very high order schemes, suffer from oscillation and unboundedness. These shortcomings were addressed through the development of the high order bounded schemes known as High Resolution (HR) schemes. A HR scheme is developed within the framework of the Normalized Variable Formulation (NVF) methodology [13] with the normalized scalar defined as

$$\tilde{\phi} = \frac{\phi - \phi_U}{\phi_D - \phi_U}, \tag{13}$$

where D represents downwind and U represents upwind grid points as in Fig. 1(a).

To make sure that the value of ϕ estimated at the face is bounded, Gaskell and Lau [16] formulated a convection boundedness criterion (CBC) for implicit, steady flow calculation. This CBC states that for a scheme to have the boundedness property, it must satisfy Eq. (14). The CBC can be visualized on a Normalized Variable Diagram (NVD) as in Fig. 1(b).

$$CBC = \begin{cases} f(\tilde{\phi}_C) & \text{is continuous,} \\ f(\tilde{\phi}_C) = 0 & \text{for } \tilde{\phi}_C = 0, \\ f(\tilde{\phi}_C) = 1 & \text{for } \tilde{\phi}_C = 1, \\ 1 < f(\tilde{\phi}_C) < \tilde{\phi}_C & \text{for } 0 < \tilde{\phi}_C < 1, \\ f(\tilde{\phi}_C) = \tilde{\phi}_C & \text{elsewhere.} \end{cases} \tag{14}$$

Any HR scheme has to fall inside the shaded triangle of Fig. 1(b), or on the first bisector outside this triangle in order to be bounded. In this work, four HR schemes are used (SMART, OSHER, MINMOD and MUSCL), and their functional relationships, given in Table 1, are presented in Fig. 1(c)–(f).

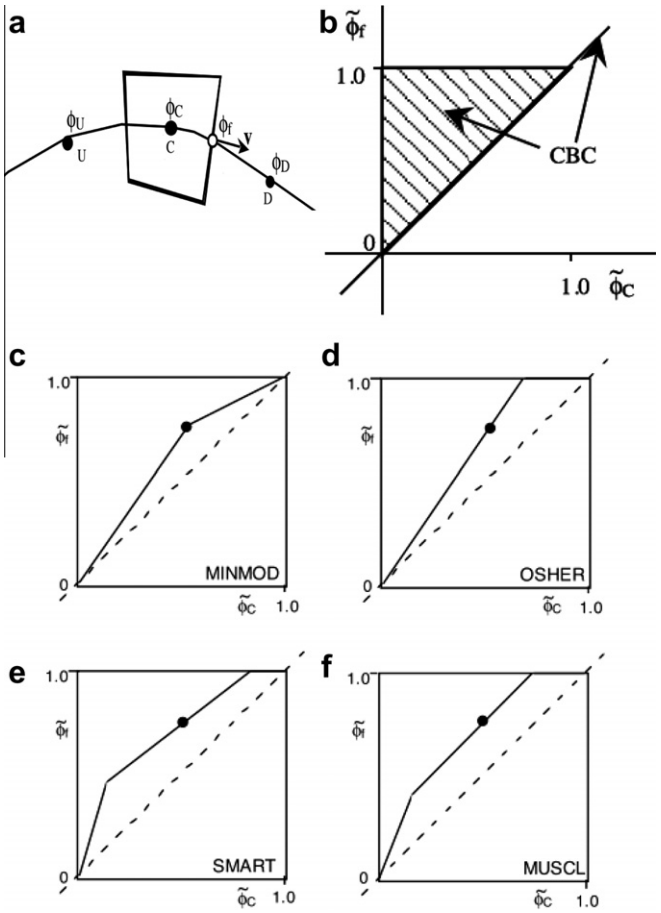

Fig. 1. (a) Control volume showing the U, C, and D locations; (b) The Normalized Variable Diagram (NVD) for the Convective Boundedness Criterion (CBC), and NVD for the (c) MINMOD, (d) OSHER, (e) SMART, and (f) MUSCL schemes.

Table 1
Functional relationship for SMART, MINMOD, MUSCL, and OSHER HR schemes.

Scheme	Functional Relationship
SMART	$\widetilde{\varphi}_f = \begin{cases} 3\widetilde{\varphi}_C & 0 < \widetilde{\varphi}_C < \frac{1}{6} \\ \frac{3}{4}\widetilde{\varphi}_C + \frac{3}{8} & \frac{1}{6} \leqslant \widetilde{\varphi}_C < \frac{5}{6} \\ 1 & \frac{5}{6} \leqslant \widetilde{\varphi}_C < 1 \\ \widetilde{\varphi}_C & \textbf{elsewhere} \end{cases}$
MINMOD	$\widetilde{\varphi}_f = \begin{cases} \frac{3}{2}\widetilde{\varphi}_C & 0 < \widetilde{\varphi}_C < \frac{1}{2} \\ \frac{1}{2}\widetilde{\varphi}_C + \frac{1}{2} & \frac{1}{2} \leqslant \widetilde{\varphi}_C < 1 \\ \widetilde{\varphi}_C & \textbf{elsewhere} \end{cases}$
MUSCL	$\widetilde{\varphi}_f = \begin{cases} 2\widetilde{\varphi}_C & 0 < \widetilde{\varphi}_C < \frac{1}{4} \\ \widetilde{\varphi}_C + \frac{1}{4} & \frac{1}{4} \leqslant \widetilde{\varphi}_C < \frac{3}{4} \\ 1 & \frac{3}{4} \leqslant \widetilde{\varphi}_C < 1 \\ \widetilde{\varphi}_C & \textbf{elsewhere} \end{cases}$
OSHER	$\widetilde{\varphi}_f = \begin{cases} \frac{3}{2}\widetilde{\varphi}_C & 0 < \widetilde{\varphi}_C < \frac{2}{3} \\ 1 & \frac{2}{3} \leqslant \widetilde{\varphi}_C < 1 \\ \widetilde{\varphi}_C & \textbf{elsewhere} \end{cases}$

The necessary condition for a scheme, derived on a uniform grid, to be second order accurate is to pass through the point Q (0.5,0.75). All schemes presented in Table 1 satisfy this condition. Moreover, a scheme is third order accurate if the derivative at Q is 0.75. It is clear that SMART is a third order accurate scheme.

In the next two sections, implementation of HR schemes using the DC and NWF methods is presented.

4.1. Deferred correction

A very simple way of implementing the HR convection scheme is by applying the DC method. In this method the convection term is initially discretized using the upwind scheme. Then, on the right hand side, an additional source term which represents the difference between the upwind and the selected HR scheme is added. In this way, the robustness of upwind is preserved, and the accuracy of the HR scheme is "deferred" to the right hand side.

Using this method, the discretized algebraic equation is written as

$$a_P^{\phi}\phi_P + \sum_{F=NB(P)} a_F^{\phi}\phi_F = b_P^{\phi} + b_P^{DC}. \tag{15}$$

The second term on the right hand side above represents the difference between the upwind and the HR scheme contribution to the convection term and is given by

$$b_P^{DC} = \dot{m}_f(\phi^U - \phi^{HR}). \tag{16}$$

Even though the left hand side is unchanged, the convergence rate diminishes upon using this method when compared to using the upwind scheme.

4.2. Normalized weighting factor

The Normalized Weighing Factor (NWF) method is based upon implicitly implementing the high-resolution convective scheme. Looking at Table 1, one can easily see that HR schemes can be cast in a general linear equation as

$$\tilde{\phi}_f = m\tilde{\phi}_C + k, \tag{17}$$

m and k are constant coefficients in every interval of $\tilde{\phi}_f$ for each HR scheme. Table 2 contains the values of m and k for the four implemented HR schemes.

The implementation of the HR scheme using NWF is a little harder than using DC. In order to implement this term, Eq. (17) is expanded and written as

$$\frac{\phi_f - \phi_U}{\phi_D - \phi_U} = m\frac{\phi_C - \phi_U}{\phi_D - \phi_U} + k, \tag{18}$$

which leads, after rearranging, to the following relation:

$$\phi_f = m(\phi_C - \phi_U) + k(\phi_D - \phi_U) + \phi_U = m\phi_C + k\phi_D + (1 - m - k)\phi_U. \tag{19}$$

Consequently, the convective flux becomes

$$J_f^C = \dot{m}_f\phi_f = \dot{m}_f \times m\phi_C + \dot{m}_f \times k\phi_D + \dot{m}_f \times (1 - m - k)\phi_U. \tag{20}$$

Table 2
Values of m and k for SMART, MINMOD, MUSCL, and OSHER HR schemes.

Scheme	Functional Relationship
SMART	$[m,k]=\begin{cases}[3,0] & 0<\widetilde{\varphi_C}<\frac{1}{6}\\ [\frac{3}{4},\frac{3}{8}] & \frac{1}{6}\leqslant\widetilde{\varphi_C}<\frac{5}{6}\\ [0,1] & \frac{5}{6}\leqslant\widetilde{\varphi_C}<1\\ [1,0] & \textbf{elsewhere}\end{cases}$
MINMOD	$[m,k]=\begin{cases}[\frac{3}{2},0] & 0<\widetilde{\varphi_C}<\frac{1}{2}\\ [\frac{1}{2},\frac{1}{2}] & \frac{1}{2}\leqslant\widetilde{\varphi_C}<1\\ [1,0] & \textbf{elsewhere}\end{cases}$
MUSCL	$[m,k]=\begin{cases}[2,0] & 0<\widetilde{\varphi_C}<\frac{1}{4}\\ [1,\frac{1}{4}] & \frac{1}{4}\leqslant\widetilde{\varphi_C}<\frac{3}{4}\\ [0,1] & \frac{3}{4}\leqslant\widetilde{\varphi_C}<1\\ [1,0] & \textbf{elsewhere}\end{cases}$
OSHER	$[m,k]=\begin{cases}[\frac{3}{2},0] & 0<\widetilde{\varphi_C}<\frac{2}{3}\\ [0,1] & \frac{2}{3}\leqslant\widetilde{\varphi_C}<1\\ [1,0] & \textbf{elsewhere}\end{cases}$

Depending on the direction of the flow, the convective term can be fully discretized and the coefficients of convection are given as

$$\begin{aligned} a_P^\phi &= \sum_{f=nb(P)} m\|\dot{m}_f,0\| - k\| - \dot{m}_f,0\|,\\ a_F^\phi &= -m\| - \dot{m}_f,0\| + k\|\dot{m}_f,0\|,\\ b_P^\phi &= \dot{m}_f(1-m-k)\phi_U. \end{aligned} \tag{21}$$

Although the authors formulated the NWF a decade ago, they have not been successful in solving the Navier Stokes equations within a segregated solver using this method. This is mainly due to the poor conditioned solution matrix. There are many cases where some diagonal entries in the matrix become negative, thus the diagonal dominance is lost. The residuals always tend to oscillate. The situation changed when the coupled solver was implemented. Results reported in [8,9] proved that the coupled solver is much more robust than SIMPLE. This motivated the authors to try using the NWF. As results in the next section will show, the NWF is successful when used within a coupled solver.

5. Results and discussion

The performance of both methods (DC and NWF) is assessed by presenting solutions to three laminar incompressible fluid flow problems: (i) lid driven flow in a square cavity, (ii) sudden expansion in a square cavity, and (iii) flow in a planar T-junction. For all problems, results are generated using three grid sizes with values of 10^4, 5×10^4, and 3×10^5 control volumes. The largest grid used was limited by the computational resources available and not because of any algorithmic limitation. The same initial guess was used for all grid sizes and computations were stopped when the maximum residual of all variables, defined as

$$\begin{cases} (\mathrm{RES})^\phi = \max\limits_{i=1}^{N} \dfrac{\left|a_P^\phi\phi_P+\sum_{F=NB(P)}a_F^\phi\phi_F-b_P^\phi\right|}{a_P^\phi\phi_{scale}},\\ \textit{where}\\ \phi_{scale} = max(\phi_{P,max}-\phi_{P,min},\phi_{P,max}) \quad \phi_{P,max}=\max\limits_{i=1}^{N}(\phi_P) \quad \phi_{P,min}=\min\limits_{i=1}^{N}(\phi_P) \end{cases} \tag{22}$$

became smaller than a vanishing quantity ε, which was set at 10^{-5}.

Results for all the grid networks used are presented in the form of the convergence history plots with tabulated values of the maximum number of iterations required and the total CPU time needed by both methods.

6. Problem 1: Lid driven flow in a square cavity

A schematic of the physical situation is depicted in Fig. 2(a). Results are presented for a value of Reynolds number (Re = ρUL/μ, L the cavity height or width, and U the axial velocity of the top horizontal wall) of 1000. Fig. 2(b) shows the streamlines in the cavity computed using the MINMOD scheme implemented following the NWF approach. Fig. 2(c) compares the pressure profile, along the horizontal centerline of the cavity, generated using the NWF and DC methods. As shown, predictions are on top of each other demonstrating the correct implementation of the methods in the coupled solver.

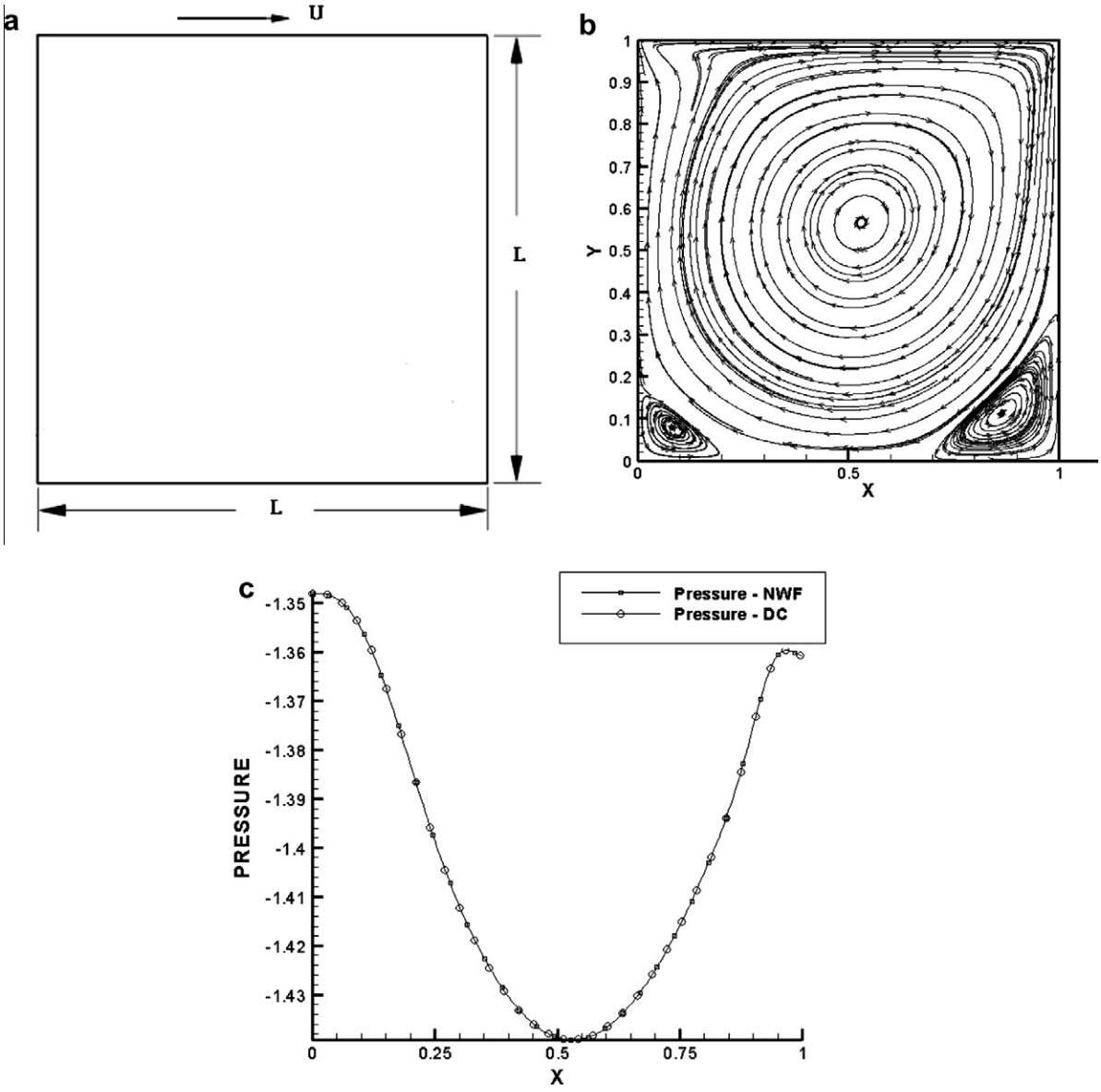

Fig. 2. (a) Physical domain and (b) Streamlines for the lid-driven flow in a square cavity problem. (c) Comparison of predicted gauge pressure along the horizontal centerline of the cavity (i.e. y = 0.5 L) using the MUSCL HR scheme implemented within the NWF and DC methods.

A summary of the number of iterations and the CPU time are presented for all grid sizes, all HR schemes, and for both the NWF and DC methods in Table 3. In addition, the table displays the percent difference in the number of iterations and CPU time between the two methods. This percentage difference is computed as

$$\%Diff = 100 \times \frac{(NWF)_{iterations\ or\ time} - (DC)_{iterations\ or\ time}}{(NWF)_{iterations\ or\ time}}. \tag{23}$$

As depicted, variation in the number of iterations is very small and with the exception of an outlier, it varies between 19 and 24 with NWF method and between 17 and 22 with the DC approach for all schemes and grid densities. For this problem, the NWF method requires slightly more iterations than the DC method. The percentage difference in the number of iterations varies between 2.9% and 22.7% with the average difference being around 16% in favor of the DC method. The same is true for the CPU time using the NWF method requiring more time to reach convergence than the DC technique. The increase in computational cost with the NWF method when compared to the DC approach varies between 2.6% and 19.3% with the average increase being around 13%. Although the NWF is fully implicit, the coefficients matrix generated by this method is not always diagonally dominant, which may negatively impact the convergence rate.

Table 3
Comparison of NWF and DC performance for the lid-driven flow problem.

HR Scheme	Grid Density	Number of iterations			CPU time		
		NWF	DC	%Diff	NWF	DC	%Diff
MINMOD	10000	24	20	+16.7	53.04	43.85	+17.3
	50000	21	17	+19.0	249.23	210.76	+15.4
	300000	19	17	+10.5	1544.1	1393.9	+9.7
MUSCL	10000	27	22	+18.5	59.61	48.08	+19.3
	50000	22	17	+22.7	254.47	209.4	+17.7
	300000	20	17	+15.0	1587.09	1436.3	+9.5
OSHER	10000	35	34	+2.9	76.95	74.96	+2.6
	50000	23	18	+21.7	277.13	223.91	+19.2
	300000	20	17	+15.0	1620.65	1362.94	+15.9
SMART	10000	24	20	+16.7	52.7	46.3	+12.1
	50000	21	17	+19.0	237	221.6	+6.5
	300000	20	17	+15.0	1693.3	1499.3	+11.5

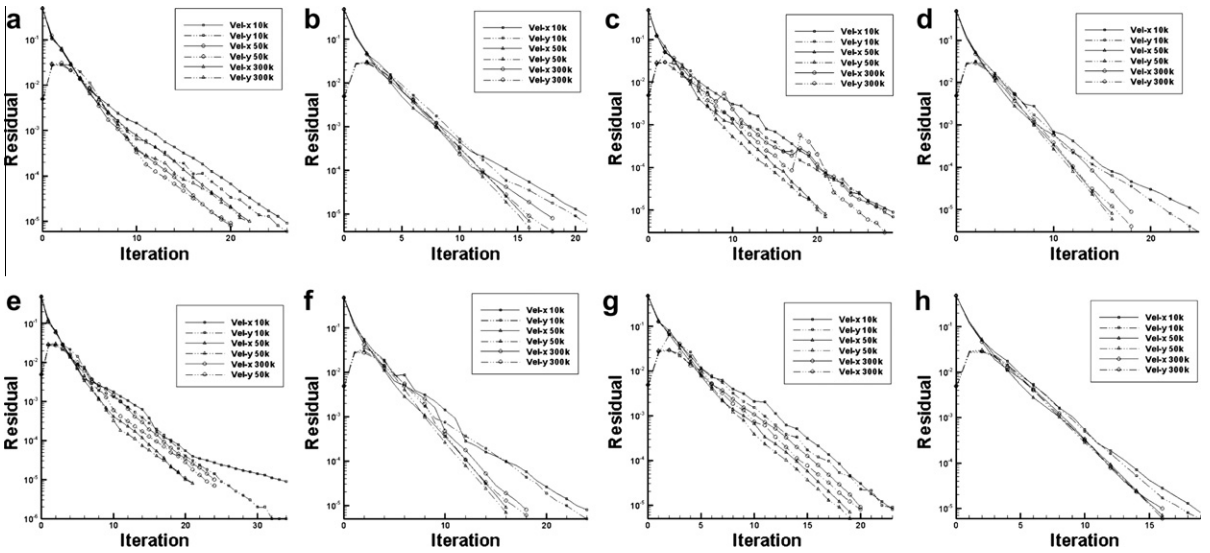

Fig. 3. Residual history plots of the lid-driven flow problem: (a) NWF–MINMOD, (b) DC–MINMOD, (c) NWF–MUSCL, (d) DC–MUSCL, (e) NWF–OSHER, (f) DC–OSHER, (g) NWF–SMART, and (h) DC–SMART.

The performance of both methods within the coupled solver is further demonstrated by the residual history plots of the momentum equations for all grid sizes presented in Fig. 3(a)–(h). Again, the plots reveal that the convergence paths in all cases are similar and the convergence rate is nearly independent of the grid size.

6.1. Problem 2: Sudden expansion in a square cavity

The physical domain is shown in Fig. 4(a) and consists of a square cavity of side L. Fluid enters the domain with a velocity $\mathbf{v}\left(\sqrt{2},\sqrt{2}\right)$ through an inlet of width $W=\frac{L}{5}$ and leaves through an opening at the top of the domain (Fig. 4(a)) also of width W. The no-slip boundary condition is applied at all walls. The problem is solved for a Reynolds number (based on the length L) of value 1000. Fig. 4(b) shows the streamlines in the cavity computed using the SMART scheme, implemented following the DC approach. Fig. 4(c) compares the pressure profile along the horizontal centerline of the cavity, generated by the MUSCL convective scheme using the NWF and DC methods. As shown, predictions are on top of each other demonstrating again, the correct implementation of the methods in the coupled solver.

Table 4 compares the number of iterations and CPU time needed by the NWF and DC methods to obtain converged solutions for all cases studied. In addition, the table displays the percentage of difference, in the number of iterations and CPU time, between the two methods. As depicted, the number of iterations varies between 22 and 35 with the NWF method and between 25 and 46 with the DC approach for all schemes and grid densities. Opposite to the previous problem, the DC method requires slightly more iterations than the NWF method. The percentage difference in the number of iterations varies

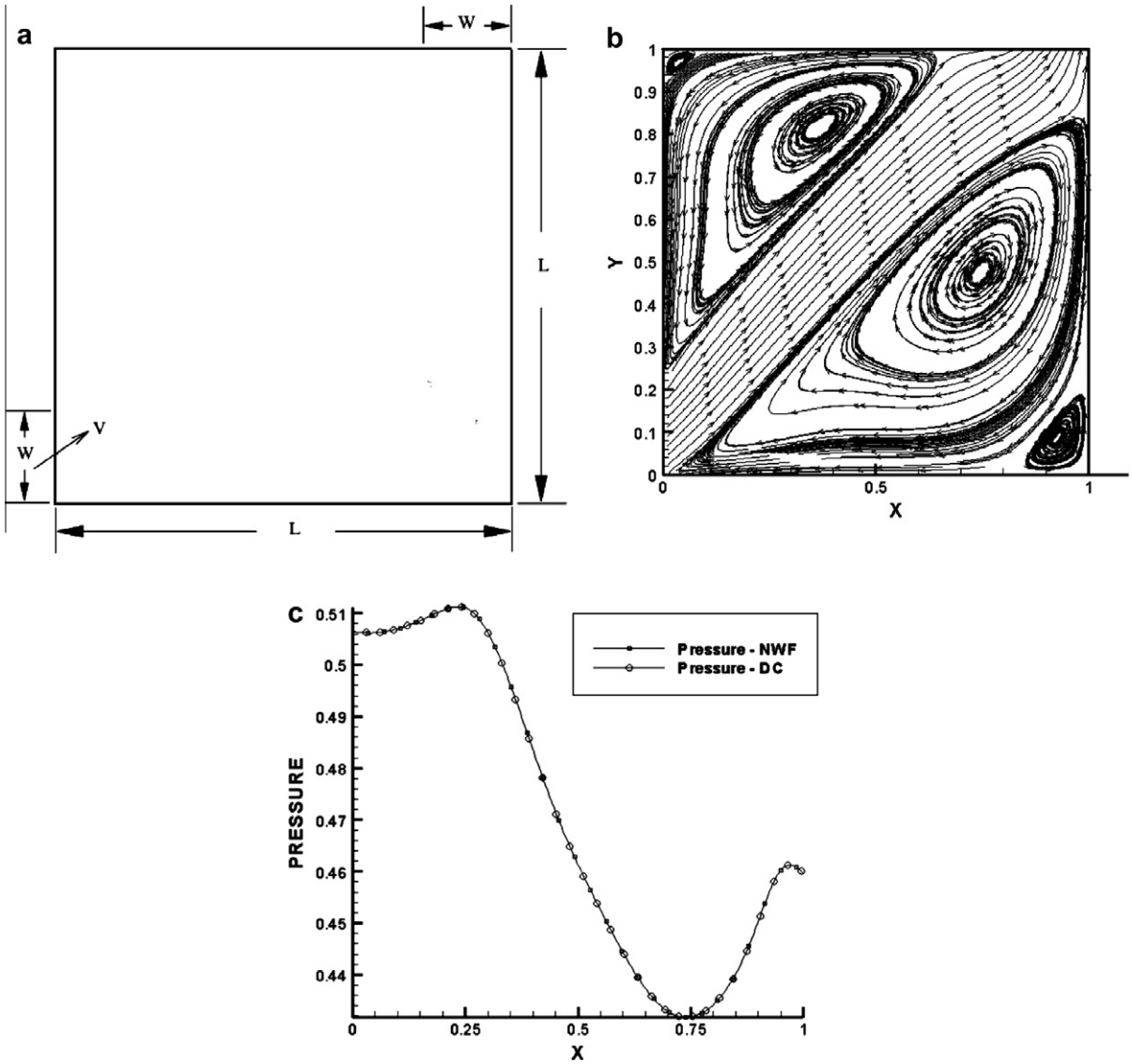

Fig. 4. (a) Physical domain and (b) streamlines for the sudden expansion flow in a square cavity problem. (c) Comparison of predicted gauge pressure along the horizontal centerline of the cavity (i.e. y = 0.5 L) using the MUSCL HR scheme implemented within the NWF and DC methods.

between −58.6% and +8.6% with the average difference being around −18.8% in favor of the NWF method. The same is true regarding the CPU time with the NWF method requiring more time to reach convergence than the DC technique. The difference in computational cost between the NWF and DC methods varies between −59.7% and +11.1% with the average increase being around −17.9% in favor of the NWF method. For this problem the performance of the NWF method is better than the DC approach.

The performance of both methods within the coupled solver is further demonstrated by the residual history plots of the momentum equations for all grid sizes presented in Fig. 5(a)–(h). Again the plots reveal that the convergence paths for all cases are similar and the convergence rate is nearly independent of the grid size.

6.2. Problem 3: Flow in a planar T-junction

The geometry of this problem is shown in Fig. 6(a). The dimensions of the domain and boundary conditions are those used by Hayes et al. [22] with the gauge pressure at the outlets set to zero. The flow enters the domain from its lower part [Fig. 6(a)] moving vertically upward with a parabolic velocity profile of $\mathbf{v}(0, 4x - 4x^2)$. The problem is solved for a Reynolds number value ($Re = \rho V_c L/\mu, V_c$ is the centerline velocity at inlet) of 1000. The width of the domain W is set at 1 m and the length L at 3 m.

Table 4
Comparison of NWF and DC performance for the sudden expansion problem.

HR Scheme	Grid Density	Number of iterations			CPU time		
		NWF	DC	%Diff	NWF	DC	%Diff
MINMOD	10000	26	31	−19.2	57.75	67.7	−17.2
	50000	24	25	−4.2	276.38	285.91	−3.4
	300000	30	30	0.0	2145.9	2289.67	−6.7
MUSCL	10000	23	32	−39.1	43.9	70.114	−59.7
	50000	22	25	−13.6	251.8	285.37	−13.3
	300000	27	30	−11.1	1894.53	2297.444	−21.3
OSHER	10000	35	32	8.6	79.05	70.247	+11.1
	50000	24	29	−20.8	277.535	332.52	−19.8
	300000	30	30	0.0	2131.65	2282.53	−7.1
SMART	10000	29	46	−58.6	72.22	101.43	−40.4
	50000	24	30	−25.0	274.21	378.8	−38.14
	300000	26	37	−42.3	1891.36	2803.44	−48.2

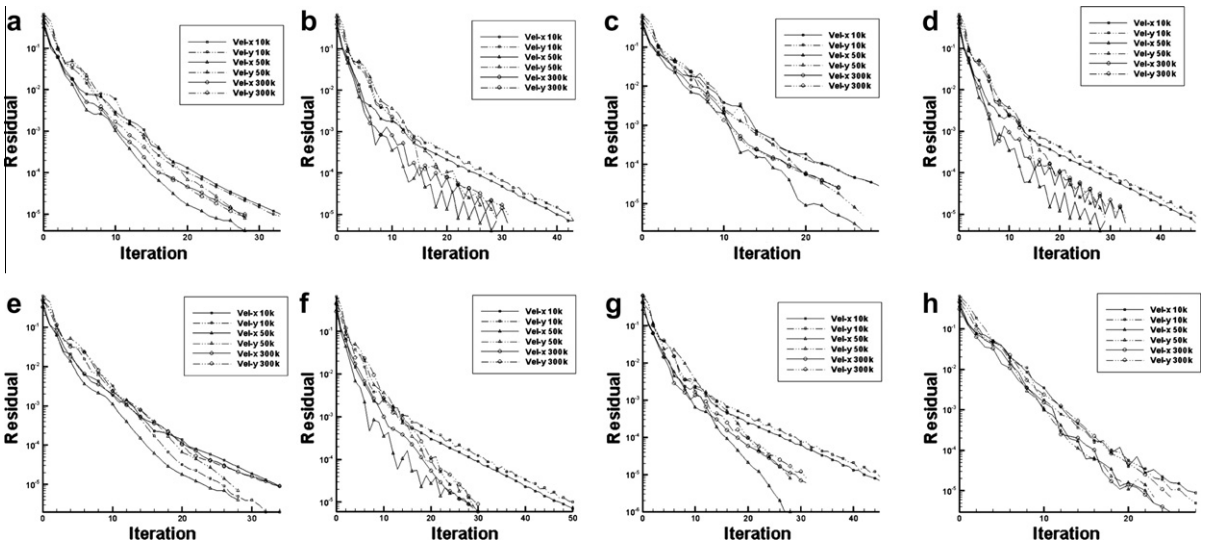

Fig. 5. Residual history plots of the sudden expansion problem: (a) NWF–MINMOD, (b) DC–MINMOD, (c) NWF–MUSCL, (d) DC–MUSCL, (e) NWF–OSHER, (f) DC–OSHER, (g) NWF–SMART, and (h) DC–SMART.

The flow field in the domain is envisaged by the streamlines presented in Fig. 6(b). As shown, the flow splits into two parts and forms a recirculation bubble at the inlet to the horizontal branch. Fig. 6(c) and (d) compare the pressure profiles at x = 0.5 m and y = 2.5 m generated using the NWF and DC methods. As shown, the two profiles in both figures fall on top of each other, giving further confirmation of the correctness of the solution methodologies.

The problem is again solved for the various grid sizes and HR schemes, and the required number of iterations and CPU time for both the DC and NWF methods are presented in Table 5. As depicted, the number of iterations required by the coupled algorithm increases with increasing the grid size although the rate of increase is small. With the NWF, the number of iterations increases from around 30 to around 80 as the grid size increases from 10^4 to 3×10^5; while for the DC method it increases from near 25 to 72 iterations. This increase is attributed to intermediate flow reversal at the exit section of the horizontal branch (Fig. 6(b)) before convergence is reached causing larger changes in the coefficients between two consecutive iterations. Similar to the first problem, the NWF method requires slightly more iterations than the DC method. The percentage difference in the number of iterations varies between 2.4% and 25.7% with the average difference being around 10.4% in favor of the DC method. The same is true regarding the CPU time, with the NWF method requiring more time to reach convergence than the DC technique. The increase in the computational cost using the NWF method when compared to the DC approach varies between 3.2% and 26.1% with the average increase being around 11%.

The convergence history plots, of the momentum equations, presented in Fig. 7(a)–(h) further reveal this performance. The increase in the number of iterations as the grid size increases is easily inferred from the plots.

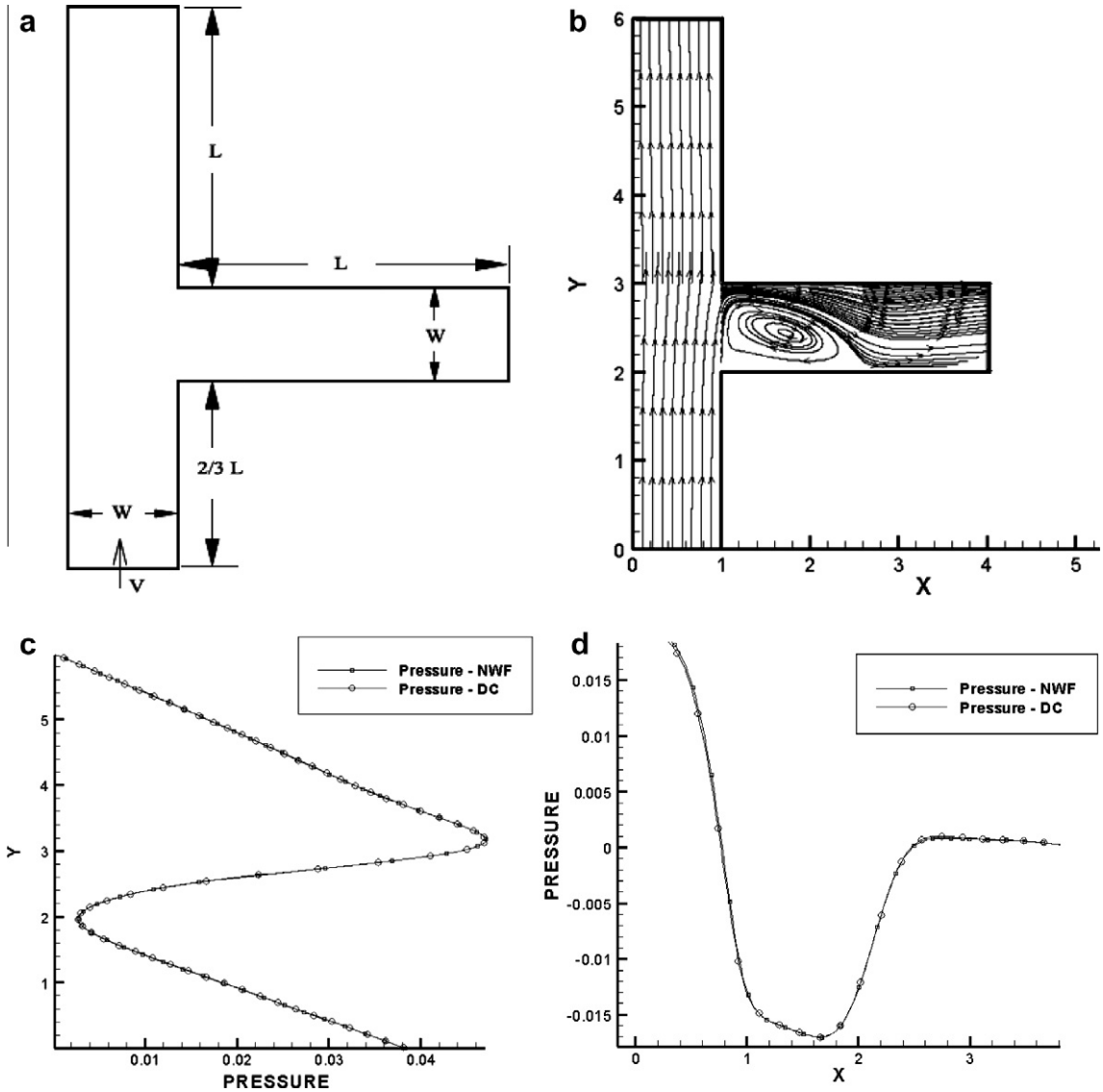

Fig. 6. (a) Physical domain and (b) streamlines for the flow in a planar T-junction problem; Comparison of predicted gauge pressure (c) at x = 0.5 and (d) at y = 2.5 using the MUSCL HR scheme implemented within the NWF and DC methods.

Table 5
Comparison of NWF and DC performance for the flow in a planar T-junction problem.

HR Scheme	Grid Density	Number of iterations			CPU time		
		NWF	DC	%Diff	NWF	DC	%Diff
MINMOD	10000	28	23	+17.9	64.4	56.96	+11.6
	50000	44	41	+6.8	524.8	483.86	+7.8
	300000	78	72	+7.7	5538.4	5171	+6.6
MUSCL	10000	33	28	+15.2	75.82	63.57	+16.2
	50000	42	41	+2.4	492.33	476.7	+3.2
	300000	75	72	+4.0	5363.3	5163.3	+3.7
OSHER	10000	33	27	+18.2	73.95	61.33	+17.1
	50000	44	41	+6.8	522.63	480.1	+8.1
	300000	77	72	+6.5	5531.5	5234.4	+5.4
SMART	10000	35	26	+25.7	79.4	58.7	+26.1
	50000	43	41	+4.7	554.94	510.7	+8.0
	300000	79	72	+8.9	2009.5	1635.6	+18.6

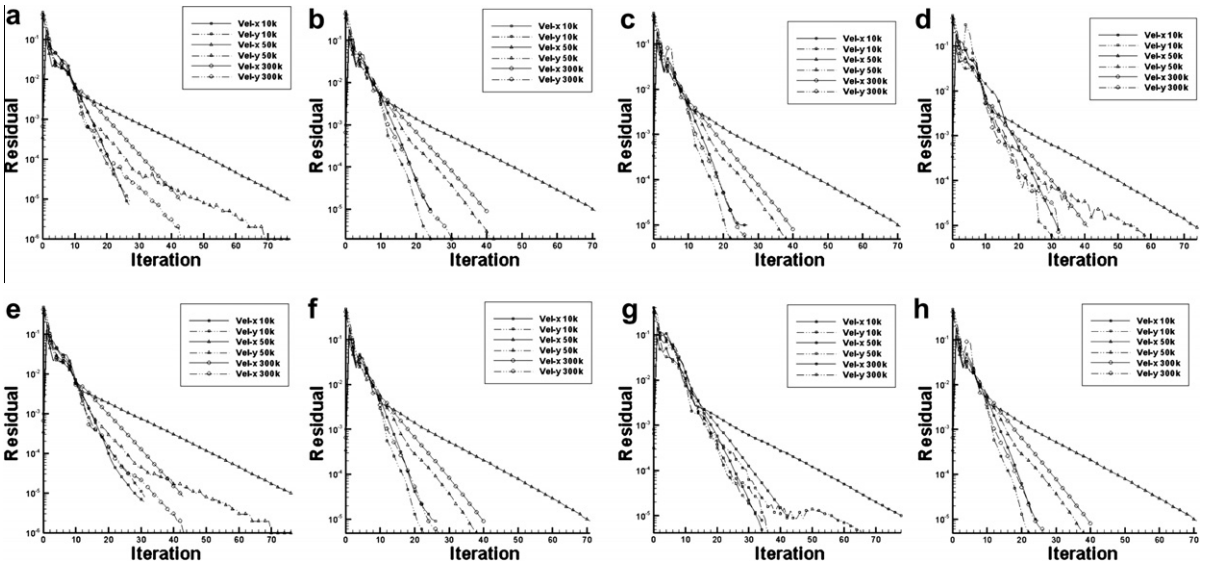

Fig. 7. Residual history plots of the flow in a planar T-Junction problem: (a) NWF–MINMOD, (b) DC–MINMOD, (c) NWF–MUSCL, (d) DC–MUSCL, (e) NWF–OSHER, (f) DC–OSHER, (g) NWF–SMART, and (h) DC–SMART.

7. Conclusion and future work

Four HR schemes were implemented in a fully coupled pressure-based flow solver, using the Normalized Weighting Factor (NWF) method and the Deferred Correction (DC) procedure. The merit of both approaches was demonstrated by comparing their computational cost in three laminar flow problems that were solved using the various HR schemes on different grid systems. Results clearly demonstrated that there is no global and consistent superiority of any method over another even though the DC method outperformed the NWF method in two out of the three test problems solved. Although the NWF did not outperform the DC method in single phase flows, it would be very interesting to check its performance within a coupled multiphase solver.

Acknowledgment

This work was supported by the University Research Board of the American University of Beirut through Grant #DDF 113040-988323.

References

[1] S.V. Patankar, D.B. Spalding, A calculation procedure for heat, mass and momentum transfer in three-dimensional parabolic flows, International Journal of Heat and Mass Transfer 15 (1972) 1787–1806.
[2] F. Moukalled, M. Darwish, A unified formulation of the segregated class of algorithms for fluid flow at all speeds, Numerical Heat Transfer, Part B 37 (1) (2000) 103–139.
[3] L.S. Caretto, R.M. Curr, D.B. Spalding, Two numerical methods for three-dimensional boundary layers, Computer Methods in Applied Mechanics and Engineering 1 (1972) 39–57.
[4] S.P. Vanka, Block-implicit multigrid solution of Navier-Stokes equations in primitive variables, Journal of Computational Physics 65 (1) (1986) 138–158.
[5] K.C. Karki, H.C. Mongia, Evaluation of a coupled solution approach for fluid flow calculations in body fitted co-ordinates, International Journal for Numerical Methods in Fluids 11 (1990) 1–20.
[6] M.E. Braaten, Development and evaluation of iterative and direct methods for the solution of the equations governing recirculating flows, PhD. Thesis, University of Minnesota, May 1985.
[7] Z. Mazhar, A procedure for the treatment of the velocity-pressure coupling problem in incompressible fluid flow, Numerical Heat Transfer, Part B 39 (2001) 91–100.
[8] M. Darwish, I. Sraj, F. Moukalled, A coupled incompressible flow solver on structured grids, Numerical Heat Transfer, Part B 52 (2007) 353–371.
[9] M. Darwish, I. Sraj, F. Moukalled, A coupled finite volume solver for the solution of incompressible flows on unstructured grids, Journal of Computational Physics 28 (1) (2009) 180–201.
[10] S. Sye, L.M. Chiapetta, A.D. Gosman, Error reduction program: final report. NASA contractor report NASA-CR-174776, 1985.
[11] W. Shyy, A study of finite difference approximations to steady state convection dominated flows, Journal of Computational Physics 57 (1985) 415–438.
[12] B.P. Leonard, A stable and accurate convective modeling procedure based on quadratic interpolation, Computer Methods in Applied Mechanics and Engineering 19 (1979) 59–98.
[13] B.P. Leonard, Simple high accuracy resolution program for convective modeling of discontinuities, International Journal for Numerical Methods in Engineering 8 (1988) 1291–1319.
[14] S.G. Rubin, P.K. Khosla, Polynomial interpolation method for viscous flow calculations, Journal of Computational Physics 27 (1982) 153–168.

[15] B.P. Leonard, S. Mokhtari, Beyond first order upwinding: the ultra-sharp alternative for non-oscillatory steady-state simulation on convection, International Journal for Numerical Methods in Engineering 30 (1990) 729–766.
[16] P.H. Gaskell, A.K.C. Lau, Curvature compensated convective transport: SMART, a new boundedness preserving transport algorithm, International Journal for Numerical Methods in Fluids 8 (1988) 617–641.
[17] M. Darwish, F. Moukalled, The normalized weighting factor method: a novel technique for accelerating the convergence of high-resolution convective schemes, Numerical Heat Transfer, Part B 30 (2) (1996) 217–237.
[18] S.R. Chakravarthy, S. Osher, High resolution applications of the OSHER upwind scheme for the Euler equations, AIAA Paper (1983) 831943.
[19] A. Harten, High Resolution Schemes for Hyperbolic Conservation Laws, Journal of Computational Physics 49 (1983) 357–393.
[20] B. Van Leer, Towards the ultimate conservative difference scheme A. A second-order Sequel to Godunov's method, Journal of Computational Physics 23 (1977) 101–136.
[21] C.M. Rhie, W.L. Chow, Numerical study of the turbulent flow past an airfoil with trailing edge separation, AIAA Journal 21 (1983) 1525–1532.
[22] R.E. Hayes, K. Nandakumar, H. Nasr-El-Din, Steady laminar flow in a 90 degree planar branch, Computers and Fluids 17 (1989) 537–553.